Available online at www.sciencedirect.com
SCIENCE DIRECT
Journal of Magnetic Resonance 181 (2006) 35–44
JMR Journal of Magnetic Resonance
www.elsevier.com/locate/jmr

Experimental validation of a $T_{2\rho}$ transverse relaxation model using LASER and CPMG acquisitions

Simona Nikolova [a,b,*], Chris V. Bowen [d], Robert Bartha [a,b,c]

[a] Imaging Research Laboratories, Robarts Research Institute, London, Ont., Canada N6A 5K8
[b] Department of Medical Biophysics, University of Western Ontario, London, Ont., Canada
[c] Department of Diagnostic Radiology and Nuclear Medicine, University of Western Ontario, London, Ont., Canada
[d] Institute for Biodiagnostics, National Research Council, Halifax, NS, Canada

Received 6 February 2006; revised 10 March 2006
Available online 17 April 2006

Abstract

The transverse relaxation rate ($R_2 = 1/T_2$) of many biological tissues are altered by endogenous magnetized particles (i.e., ferritin, deoxyhemoglobin), and may be sensitive to the pathological progression of neurodegenerative disorders associated with altered brain-iron stores. R_2 measurements using Carr–Purcell–Meiboom–Gill (CPMG) acquisitions are sensitive to the refocusing pulse interval ($2\tau_{cp}$), and have been modeled as a chemical exchange (CE) process, while R_2 measurements using a localization by adiabatic selective refocusing (LASER) sequence have an additional relaxation rate contribution that has been modeled as a $R_{2\rho}$ process. However, no direct comparison of the R_2 measured using these two sequences has been described for a controlled phantom model of magnetized particles. The three main objectives of this study were: (1) to compare the accuracy of R_2 relaxation rate predictions from the CE model with experimental data acquired using a conventional CPMG sequence, (2) to compare R_2 estimates obtained using LASER and CPMG acquisitions, and (3) to determine whether the CE model, modified to account for $R_{2\rho}$ relaxation, adequately describes the R_2 measured by LASER for a full range of τ_{cp} values. In all cases, our analysis was confined to spherical magnetic particles that satisfied the weak field regime. Three phantoms were produced that contained spherical magnetic particles (10 μm diameter polyamide powders) suspended in Gd-DTPA (1.0, 1.5, and 2.0 mmol/L) doped gel. Mono-exponential R_2 measurements were made at 4 T as a function of refocusing pulse interval. CPMG measurements of R_2 agreed with CE model predictions while significant differences in R_2 estimates were observed between LASER and CPMG measurements for short τ_{cp} acquisitions. The discrepancy between R_2 estimates is shown to be attributable to contrast enhancement in LASER due to $T_{2\rho}$ relaxation.

Keywords: R_2; $T_{2\rho}$; LASER; Chemical exchange; Weak field regime

1. Introduction

The degree of magnetic induction within biological tissue placed in an external magnetic field is described by the magnetic susceptibility (χ) and depends on the composition of the tissue. For example, certain metal elements found in tissue (e.g., iron) have an inherently high magnetic susceptibility relative to water or air and experience pronounced magnetization when placed in an external field. Variations in stored iron (ferritin) concentration [1,2] and deoxyhemoglobin concentration in red blood cells [3], cause regional magnetic susceptibility differences in tissues of the brain [4,5] and liver [6], which can lead to a reduction in the measured transverse relaxation rate ($R_2^{\dagger}$) in these tissues. Since neurodegenerative conditions such as Parkinson's, Huntington's, and Alzheimer's disease involve altered brain-iron concentrations [7], and hereditary hemochromatosis [6] involves iron overload in the liver, quantitative R_2 measurements to assess tissue iron concentration could be used to identify and monitor the pathologic progression of these conditions.

* Corresponding author. Fax: +1 519 663 3078.
E-mail address: Nikolova@imaging.robarts.ca (S. Nikolova).

1090-7807/$ - see front matter © 2006 Elsevier Inc. All rights reserved.
doi:10.1016/j.jmr.2006.03.013

The most common imaging techniques used for the measurement of R_2 relaxation rate time constants are the single-echo spin-echo (Hahn echo) [8] pulse sequence and the Carr–Purcell–Meiboom–Gill (CPMG) sequence [9,10] involving multi-echo spin-echo acquisitions. With CPMG measurements, an initial 90° excitation pulse is followed by multiple, non-adiabatic, 180° refocusing pulses prior to data acquisition. Local variations in tissue susceptibility produce microscopic regions having different magnetic field strength that alter CPMG measurements of R_2 through dynamic averaging (DA) [11]. This process describes the loss of phase coherence in the refocused magnetization that occurs through either the diffusion or exchange of spins between regions having different magnetic field strength and is sensitive to the refocusing pulse interval. Many MR imaging techniques have exploited magnetic susceptibility variations to produce images with enhanced DA contrast [12–15].

Recently, Garwood and DelaBarre [16] developed the LASER multi-echo spin-echo spectroscopic localization sequence for biological applications. This sequence combines high bandwidth adiabatic radiofrequency (RF) pulses with slice select gradients to produce sharper voxel profiles than those obtained with conventional RF pulses [16]. LASER can also be used to measure the transverse relaxation rate ($R_2^\dagger$) [17,18] in localized volumes and generate DA contrast related to differences in microscopic susceptibility in localized tissue regions [18]. Dynamic averaging is manipulated by varying the number and time between adiabatic pulses in a Carr–Purcell (CP) pulse train incorporated into the LASER pulse sequence. Using an adiabatic CP-type sequence, Kavec et al. [19] observed unique DA contrast in post-stroke brain tissue. In addition to dynamic averaging, the generation of rotating frame transverse relaxation contrast ($T_{2\rho}$) was demonstrated by Michaeli et al. [11,20] in a CP spin-echo sequence consisting of a series of hyperbolic secant (HSn) adiabatic full passage pulses, with no delay between pulses.

The rate of decay of the transverse NMR signal in biological tissue from DA has often been described as an exchange process using a two-site chemical exchange model [21,22], with an exchange time (τ_{ex}) and frequency difference ($\Delta\omega_{ab}$) between the two exchanging sites [21]. The influence on R_2 of particles with high magnetic susceptibility dispersed within tissue can be considered in the weak field regime when $\tau_{ex} < \Delta\omega_{ab}^{-1}$. The weak field approximation has been used to describe systems including red blood cells, non-heme iron containing cells within white or gray matter, and liver hepatocytes [2,8,12]. A theoretical model has been proposed [21] to describe the variation in the transverse relaxation rate (R_2) with refocusing pulse interval ($2\tau_{cp}$) in the weak field regime. In this model, Brooks et al. [21] integrated quantum outer sphere relaxation theory and classical mean gradient diffusion theory, and showed that chemical exchange (CE) theory [23] provides a good approximation to both theories. This model, which is referred to as the CE model, was tested by Brooks et al. [21] using Monte Carlo simulations for spherical particles, however in vitro or in vivo experimental validation was not provided. Alternatively, a theoretical model proposed by Jensen and Chandra [24] describing DA contrast resulting from a diffusion process predicts the variation of R_2 in the weak field regime as a function of τ_{cp}. However, this model is more computationally intensive and less well established than the CE model, and therefore the current analysis will be restricted to the CE model only. Although the CE model provides a description of the instantaneous relaxation rate that occurs during the time between refocusing pulses, Michaeli et al. [11,20] describe the transverse relaxation that occurs in the rotating frame ($T_{2\rho}$) during application of the adiabatic refocusing pulse with predictions that consider both contributions described for the measured transverse relaxation time constant ($T_2^\dagger$) in adiabatic CP sequences.

The use of $T_2^\dagger$ (or $R_2^\dagger$) mapping techniques has the potential to quantify endogenous or exogenous contrast agents that generate microscopic susceptibility gradients in medical imaging applications. However, validation of the CE theory and contributions from $T_{2\rho}$ relaxation during application of adiabatic pulses has not been previously demonstrated in vitro for a controlled phantom model of magnetized particles. Therefore, the three goals of this study were: (1) to compare the accuracy of R_2 relaxation rate predictions from the CE model with experimental data acquired using a conventional CPMG sequence, (2) to compare R_2 relaxation rates measured using the LASER pulse sequence to those acquired using the CPMG sequence, and (3) to determine whether the CE model, modified to account for $T_{2\rho}$ (or $R_{2\rho}$) relaxation, adequately describes the R_2 relaxation rates measured using LASER for short τ_{cp} acquisitions. In all cases, our analysis was confined to spherical magnetic perturbers satisfying the weak field regime ($\tau_{ex} < \Delta\omega_{ab}^{-1}$) using phantoms containing microsphere particles suspended in Gd-DTPA doped gel.

2. Theory

Media containing dispersed weak magnetic particles can be modeled as a system with two distinct compartments, each having a different magnetic susceptibility. The diffusion of spins exterior to the particle compartment produces a transverse relaxation rate (R_2) that is dependent on the temporal correlation function of the field inhomogeneities experienced by a diffusing spin. Brooks et al. [21] proposed to use the expression obtained by Luz and Meiboom [23] describing relaxation (R_2) due to exchange between compartments having chemical shift frequency offset $\Delta\omega_{ab}$ to account for relaxation induced by a diffusion process:

$$R_2 = R_{20} + R_{2D}\left[1 - \frac{\tau_{ex}}{\tau_{cp}}\tanh\left(\frac{\tau_{cp}}{\tau_{ex}}\right)\right], \quad (1)$$

where R_{20} indicates the relaxation rate of a sample having no magnetic particles, τ_{ex}—the exchange time between

compartments having chemical shift frequency offset $\Delta\omega_{ab}$, $R_{2D} = F_a F_b \Delta\omega_{ab}^2 \tau_{ex}$, the maximum potential relaxation enhancement due to the presence of magnetic particles for a given exchange time, τ_{ex} and F_a, F_b are the fraction of protons in the interior and exterior compartments, respectively.

Brooks et al. [21] extended this model to provide exact relaxation rate estimates in the presence of magnetized spheres by comparing predictions from classical diffusion and quantum outer sphere relaxometry theory with those of CE theory. In their work, asymptotic solutions of the CE model in the short ($\tau_{cp} \ll \Delta\omega_{ab}^{-1}$) and long ($\tau_{cp} \gg \Delta\omega_{ab}^{-1}$) echo domain were compared with predictions from classical diffusion and quantum outer sphere relaxometry theories, respectively. This approach led to CE model parameter definitions that were appropriate in the weak field regime for magnetized particles. The relationship between the two-site exchange equation parameters of the CE model (F_a, F_b, τ_{ex}, $\Delta\omega_{ab}$), and the physical parameters of a suspension of magnetized particles (v, τ_d, $\Delta\chi_{ab}$) are as follows:

$$F_a = 1.7v \quad \text{and} \quad F_b = 1 - F_a, \tag{2a}$$

$$\tau_{ex} = 0.26\tau_d, \tag{2b}$$

$$\Delta\omega_{ab} = \sqrt{\frac{4}{5}}\gamma B_e, \text{ where } B_e = \frac{\Delta\chi_{ab} B_0}{3}, \tag{2c}$$

where v is the volume fraction occupied by the particles, $\tau_d = r^2/D$, with D being the diffusion suspension media self-diffusion coefficient, and r is the particle radius. B_e is the equatorial magnetic field, $\Delta\chi_{ab}$ is the susceptibility offset of the spherical particles from the suspension media in SI units, and B_0 is the static magnetic field strength. The relations given by Eq. (2) are valid for a low volume fraction of magnetic particles. Monte Carlo simulations of spherical particles were previously used to validate the theory [25].

Michaeli et al. [11] suggested a modified expression for the transverse relaxation rate ($R_2^\dagger$) associated with an adiabatic full passage CP pulse sequence. The modified general expression for $R_2^\dagger$ incorporating a term due to the presence of transverse relaxation in the rotating frame was shown to be [11]:

$$R_2^\dagger = \{R_{2\rho} - R_2\}\frac{T_p}{2\tau_{cp}} + R_2, \tag{3}$$

where R_2 indicates the relaxation rate predicted by the CE model (Eq. (1)) that occurs between adiabatic refocusing pulses, $R_{2\rho}$ indicates the transverse relaxation component in the rotating frame that occurs during application of adiabatic refocusing pulses, and T_p is the duration of the adiabatic refocusing pulse. Eq. (3) shows that without time delays between refocusing pulses ($T_p = 2\tau_{cp}$), the measured relaxation rate is governed by $R_{2\rho}$. Michaeli et al. [11] have proposed a model for estimating $R_{2\rho}$ that consists of a term representing the exchange induced transverse relaxation rate ($R_{2\rho,ex}$) and a term representing the dipolar interactions ($R_{2\rho,dd}$) as follows:

$$R_{2\rho} = \frac{1}{T_p}\int_0^{T_p} R_{2\rho,ex}(t)\,dt + \frac{1}{T_p}\int_0^{T_p} R_{2\rho,dd}(t)\,dt. \tag{4}$$

Both $R_{2\rho,ex}$ and $R_{2\rho,dd}$ vary instantaneously and are functions of the specific amplitude and phase modulation of the refocusing pulse employed. In the case of magnetized particles, the exchange term $R_{2\rho,ex}$ is a function of the physical parameters of the suspension of magnetized particles and the adiabatic refocusing pulse according to the equation [11]:

$$R_{2\rho,ex} = F_a F_b (\Delta\omega_{ab})^2 \cos^2\alpha\tau_{ex}, \tag{5}$$

where α is the instantaneous angle between B_0 and the effective field of the adiabatic refocusing pulse, and F_a, F_b, $\Delta\omega_{ab}$, and τ_{ex} are as described in Eq. (2). Only the first term in Eq. (4) describing exchange induced relaxation is a function of the susceptibility offset between the magnetic particles and the suspension, and varies with the square of Gd-DTPA concentration for our phantom model.

The current study directly compared transverse relaxation rate measurements obtained with the CPMG (R_2) and LASER ($R_2^\dagger$) pulse sequences in phantoms containing small volume fractions of spherical magnetic particles. All phantoms were prepared to satisfy the weak field regime condition ($\tau_{ex} < \Delta\omega_{ab}^{-1}$) and results were compared with the predictions of CE theory (Eq. (1)). Differences in the transverse relaxation rates obtained from each pulse sequence were used to estimate $R_{2\rho}$ for each phantom using Eq. (3), and the results were compared with theoretical predictions for LASER acquisitions as described in Eqs. (4) and (5).

3. Methods

3.1. Phantom design

The effect of microscopic susceptibility-induced field inhomogeneities on the transverse relaxation rate was investigated using phantoms containing ORGASOL® (ATOFINA Canada Inc., Ont., Canada) microbeads (polymers of lauryllactame and caprolactame obtained by direct polymerization). The ORGASOL® beads are spherical particles available in a range of sizes having a narrow particle size distribution (particle diameter has 3 μm standard deviation). Phantom solutions were created in 50 ml cylindrical culture tubes containing a 10% volume fraction of ORGASOL® (density 1.07 g/L), 5% agarose gel, 100 mM NaCl (for RF coil loading), and 33% Photo-Flo (*p-tertiary*-octylphenoxy polyethyl alcohol). The surfactant, Photo-Flo (Eastman Kodak Company, Rochester, NY) was used to minimize air bubble formation within the mixture, while the agarose gel prevented sedimentation of the microbeads. A diffusion coefficient of 2.1×10^{-3} mm^2/s was measured in our phantoms using a standard spin-echo diffusion weighted imaging sequence with a range of 7 applied b values (0, 9, 38, 85, 151, 236, 340 s/mm^2). Phantoms were continuously rotated during gel cooling and solidification to maintain a homogeneous microbead distribution.

Three phantoms were designed with different transverse relaxation rates by mixing the contrast agent Gd-DTPA into the microbead suspensions to produce a susceptibility offset between the microbead and gel compartments. Phantoms were designed to satisfy two criteria: (1) the microbead size was selected to produce a τ_{ex} value intermediate to the achievable range of τ_{cp} values for the LASER sequence (using Eq. (2b)); and (2) Gd-DTPA concentrations were selected to produce R_2 values that spanned values as large as the inverse of the minimum possible echo time. The second criterion was satisfied using Eqs. (1) and (2) and the result of two calibrations described in the sections below. Calibration of both the measured relaxation rate (R_{20}) and the gel sample bulk magnetic susceptibility offset referenced to water ($\Delta\chi_s$) for variation in sample Gd-DTPA concentration was obtained using phantoms without microbeads. Table 1 lists the particle size and the Gd-DTPA concentrations used in each bead suspension phantom.

3.2. Relaxation rate measurements

Experiments were performed using a 4 T whole body MR scanner, consisting of an Oxford Magnet Technology (OMT) 90 cm magnet, Varian Unity INOVA console, and Siemens Sonata gradient system. A non-localized CPMG pulse sequence was used for R_2 measurement in which the refocusing pulse interval ($2\tau_{cp} = 5.0$–12.5 ms, in steps of 0.5 ms) was set to correspond to the time between the adiabatic full passage (AFP) pulses in the LASER sequence (described below). Since 180° pulses in CPMG are self-refocusing while echo formation with LASER requires pairs of AFP pulses, 16 echoes were acquired with CPMG spanning a similar range of echo times (TE from 10 to 160 ms) as the 7 echoes with LASER (TE from 30 to 150 ms). The CPMG measurements were performed for each phantom in the same scan session as the LASER acquisitions. A set of 16 spectra corresponding to a linearly spaced range of echo times (TE from 10 to 160 ms) was obtained for CPMG acquisitions.

The LASER pulse sequence [16] used for all relaxation rate measurements employs a non-selective adiabatic half passage (AHP) excitation pulse followed by six slice selective HS2-R15 [26] refocusing pulses for 3D volume selection. Additional non-selective HS1-R10 [27] MLEV phase cycled [28] (AFP) pulses were applied prior to the slice selective pulses to extend the target echo time (TE), while maintaining a constant time between AFP pulses ($2\tau_{cp}$). Voxel localized spectra (18 averages, TR = 4 s, 2 kHz receiver bandwidth) were acquired from a voxel ($18 \times 18 \times 25$ mm^3) positioned completely within each phantom (Fig. 1) for $R_2^{\dagger}$ measurements using 16 different refocusing pulse intervals ($2\tau_{cp} = 5.0$–12.5 ms, in steps of 0.5 ms). For each τ_{cp} value, spectra were acquired at seven different, linearly spaced echo times (TE from 30 to 150 ms) corresponding to the addition of 0, 4, 8, 12, 16, 20, and 24 non-selective refocusing pulses (Fig. 1). Mono-exponential least squares regression fits of the maximum amplitude of the echoed time domain signal (peak area in the frequency domain), obtained at each echo time (TE), were used to estimate transverse relaxation rates for each pulse sequence.

Table 1
CE model predictions

Phantom	Particle radius (μm)	Gd-DTPA (mM/L)	Photo-Flo (ml)	$\Delta\omega_{ab}$ (rad s^{-1})[a]	τ_{ex} (ms)[b]	R_{20} (s^{-1})[c]	R_{2D} (s^{-1})[d]
1	5	1	20	145	3.1	16.90	10.2
2	5	1.5	20	193	3.1	20.14	17.8
3	5	2	20	240	3.1	23.25	27.7

[a] Calculated using Eq. (2c) with $\Delta\chi_{ab}$ calibration from Eq. (7).
[b] Calculated using Eq. (2b) with $D = 2.1 \times 10^{-3}$ mm^2/s.
[c] From Eq. (6) using CPMG relaxivity calibration parameters.
[d] Calculated using Eqs. (1) and (2).

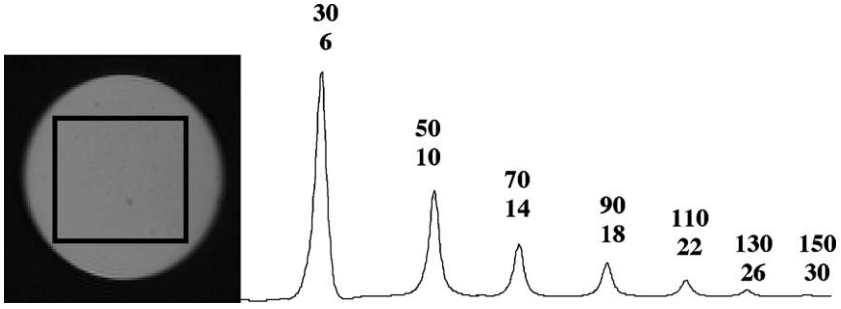

Fig. 1. Transverse image of phantom #3 (left) with the chosen voxel ($18 \times 18 \times 25$ mm^3) superimposed. Typical spectra obtained by insertion of 0, 4, 8, 12, 16, 20, and 24 MLEV pulses prior to the six LASER localization pulses. Signal intensity decreases as the number of pulses (echo time) increases. The spectra shown were obtained with $2\tau_{cp} = 12.5$ ms. The numbers above each spectrum represent the echo time in ms (top), and the total number of AFP pulses used in the acquisition of each spectrum (bottom).

3.3. Gd-DTPA relaxivity and magnetic susceptibility calibrations

The parameter R_{20} in Eq. (1) represents the relaxation rate of the sample without microbeads and depends on the concentration of both Gd-DTPA and Photo-Flo. The relaxation rate varies linearly with Gd-DTPA concentration in the following manner:

$$R_{20} = c[\mathrm{Gd}] + y, \tag{6}$$

where the parameter c represents the R_2 relaxivity of Gd-DTPA, [Gd] refers to the concentration of Gd-DTPA in mmol, and y represents the relaxation rate in a sample from all mechanisms other than paramagnetic relaxation by Gd-DTPA. The established literature value for the relaxivity (c) in Eq. (6) of Gd-DTPA is roughly 6 L mmol^{-1} s^{-1} [29] for measurements made at field strengths between 0.5 and 1.5 T. The relaxivity of Gd-DTPA was measured by preparing phantoms with a range of Gd-DTPA concentrations (0, 0.1, 0.4, 0.6, 1, 2, 3, 4, 6, 8 mM). R_{20} was measured with the CPMG pulse sequence for each phantom at the minimum achievable refocusing pulse interval ($2\tau_{cp} =$ 5.0 ms) using sixteen echo times as described above. Similarly, R_{20} was calibrated with the above mentioned Gd-DTPA concentrations using the LASER pulse sequence. The minimum achievable time between AFP pulses ($2\tau_{cp} = 5.0$ ms) was used with seven echo times, as described above. A linear regression of R_{20} estimates was used to estimate c and y in Eq. (6) for both LASER and CPMG pulse sequences.

Susceptibility measurements were performed to determine the susceptibility difference ($\Delta\chi_{ab}$) between the two compartments present within each microbead suspension phantom. The measurement of susceptibility difference was essential for a proper comparison of measured relaxation rates to the predictions of theoretical models. An imaging based form of MR susceptometry, previously described in detail [30,31], was used to determine the sample susceptibility difference referenced to water ($\Delta\chi_s$). Briefly, the susceptometry apparatus consisted of a 5 mm outer diameter NMR tube placed concentrically (using teflon spacers), within a 15 mm inner diameter, 10-ml graduated cylinder. The graduated cylinder contained distilled water and the surfactant Photo-Flo to inhibit bubble formation. The apparatus was placed vertically within a 5 cm diameter solenoid RF coil. Axial images of the phantom were acquired using a 2D multi-echo gradient echo sequence (128×128 matrix, 10 mm slice, 6 cm FOV, 8 ms echo spacing, 20 echoes). The susceptibility-induced field inhomogeneity pattern was characterized outside of the NMR tube oriented perpendicular to B_0. The field inhomogeneity pattern was determined by generating a field map from the evolution of phase with echo time. By fitting the field inhomogeneity pattern outside the NMR tube, but within the graduated cylinder, to the theoretical field pattern for co-axial cylinders [32], the susceptibility of the sample within the NMR tube, referenced against that of water ($\Delta\chi_{ab}$) was estimated [30].

The water referenced susceptibility of the ORGASOL® polystyrene beads was obtained by measuring the susceptibility ($\Delta\chi_b$) of a high density microbead sample containing 0.5 g of 20 μm diameter ORGASOL®, 33% Photo-Flo, and 1 ml of water (32% volume fraction of polystyrene beads in sample). The bead susceptibility ($\Delta\chi_b$) referenced to water was found to be -0.157 ± 0.004 ppm in SI units ($\Delta\chi_b = \Delta\chi_{ab}/0.32$, where 0.32 represents the volume fraction). The water referenced susceptibility of Gd-DTPA in agarose gel ($\Delta\chi_{Gd}$) was calibrated by measuring $\Delta\chi_s$ in four 5% w/w agarose phantoms, containing a range of Gd-DTPA concentrations (0, 1, 2, and 4 mmol) and no microbeads. The compartmental susceptibility offset ($\Delta\chi_{ab}$) for phantoms containing polystyrene beads suspended in Gd doped agarose was then determined using $\Delta\chi_{ab} = \Delta\chi_{Gd} - \Delta\chi_b$.

3.4. Data analysis

Plots of signal intensity vs. echo time were produced for each phantom at 16 different pulse intervals ($2\tau_{cp} = 5.0$–12.5 ms, step 0.5 ms). The MR signal decay in both CPMG and LASER experiments was characterized using the maximum amplitude of the echoed time domain signal obtained at each echo time, using MATLAB (The Mathworks Inc., Natick, MA, USA). R_2 and $R_2^\dagger$ estimates were obtained from the signal intensity decay curves of CPMG and LASER measurements, respectively, using a three parameter (S_0, R_2, and B) constrained least squares regression with the functional form ($S = S_0 \cdot \exp(-R_2 \cdot TE) + B$). For each microsphere suspension phantom (Table 1), the τ_{cp} dependence of the measured R_2 estimates obtained from CPMG measurements were fit using the CE model. Chemical exchange model parameters were obtained using a three parameter (R_{20}, R_{2D}, and τ_{ex}) constrained least squares regression of Eq. (1) in MATLAB. In each case, fitting was performed using a variance normalized regression kernel [33], where the variance of the R_2 parameter ($\sigma^2(R_2)$) was estimated, for each τ_{ex} value, from the fit residuals of the mono-exponential signal decay curve.

The contribution of transverse relaxation in the rotating frame, $R_{2\rho}$, was estimated for each phantom from differences in the τ_{cp} dependence of the transverse relaxation measurements obtained from LASER ($R_2^\dagger$) and CPMG (R_2) acquisitions, as described in Eq. (3). A single parameter constrained least squares regression estimate of $R_{2\rho}$ was obtained using the inverse fractional adiabatic pulse time ($2\tau_{cp}/T_p$) as the variance normalization kernel, since $R_{2\rho}$ estimates are most reliable for short τ_{cp} acquisitions.

4. Results

4.1. Gd-DTPA relaxivity and susceptibility calibration measurements

The slope (c) and intercept (y) of the Gd-DTPA transverse relaxivity calibration (Eq. (6)) were found to be

6.65 ± 0.73 L mmol^{-1} s^{-1} and 10.65 ± 1.57 s^{-1}, respectively, when measured with the CPMG pulse sequence, and 7.26 ± 0.45 L mmol^{-1} s^{-1} and 11.83 ± 0.98 s^{-1}, respectively, when measured with the LASER pulse sequence. Phantoms without beads and containing 33% of Photo-Flo were used for calibration with each pulse sequence. Relaxivity calibration parameter estimates obtained using each sequence differed by less than 10% and agreed within uncertainty for both c and y ($p = 0.48$ and 0.52, respectively). The water referenced susceptibility of Gd-DTPA measured by susceptometry was 0.299 ppm/mM. Therefore, the relationship between the susceptibility offset between compartments ($\Delta\chi_{ab}$) of bead suspension phantoms, and the Gd-DTPA concentration of the suspension gel was expressed as:

$$\Delta\chi_{ab} = 0.299[\mathrm{Gd}] + 0.16, \quad (7)$$

where [Gd] is the concentration of Gd-DTPA in mM, and –0.16 ppm is the water referenced susceptibility offset of the polystyrene microbeads ($\Delta\chi_b$).

4.2. R_2 measurements

Fig. 1 shows typical spectra acquired from phantom 3 (see Table 1) as a function of echo-time using the LASER pulse sequence. The observed spectra exhibited a single resonant peak and signal intensity diminishing with echo time. Figs. 2A and B show semi-log plots of the spectral area as a function of the echo time (TE) in all phantoms, obtained with the LASER and CPMG pulse sequences, respectively. All semi-log signal decay fits produced very high correlation coefficients ($R^2 > 0.99$) supporting the assertion of mono-exponential decay, characterized by R_2 and $R_2^\dagger$ for CPMG and LASER acquisitions, respectively. The results from Figs. 2A and B were obtained with $2\tau_{cp} = 5.0$ ms, however comparable linearity was observed for acquisitions involving all other refocusing pulse intervals (data not shown).

Figs. 3A–C shows the τ_{cp} dependence of R_2 and $R_2^\dagger$ estimates for all bead suspension phantoms with corresponding fits to the CE model (Eq. (1)) using data acquired with the CPMG and LASER pulse sequences, respectively. CE model parameter estimates (τ_{ex}, R_{20}, R_{2D}) of the R_2 variation shown in Fig. 3 are listed in Table 2 for CPMG acquisitions alone, since CE model predictions are only valid for CPMG acquisitions. Table 1 lists theoretical predictions for τ_{ex}, and R_{2D} derived from the physical properties of the phantom, and Eqs. (1) and (2) (CE model). The value of R_{20} predicted from calibration measurements using phantoms without microspheres is also indicated. Parameter estimates listed in Table 2 for CPMG data were in close

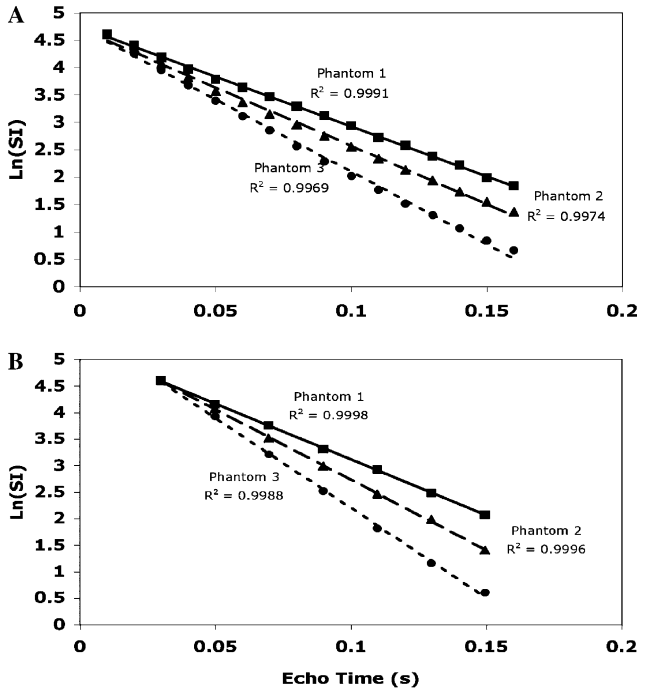

Fig. 2. Semi-log plot of spectral area as a function of echo time (TE) for all microsphere suspension phantoms ($2\tau_{cp} = 5.0$ ms) acquired with (A) the CPMG pulse sequence, (B) the LASER pulse sequence. The R_2 and $R_2^\dagger$ relaxation rates were determined from the slopes of each regression line in (A) and (B), respectively.

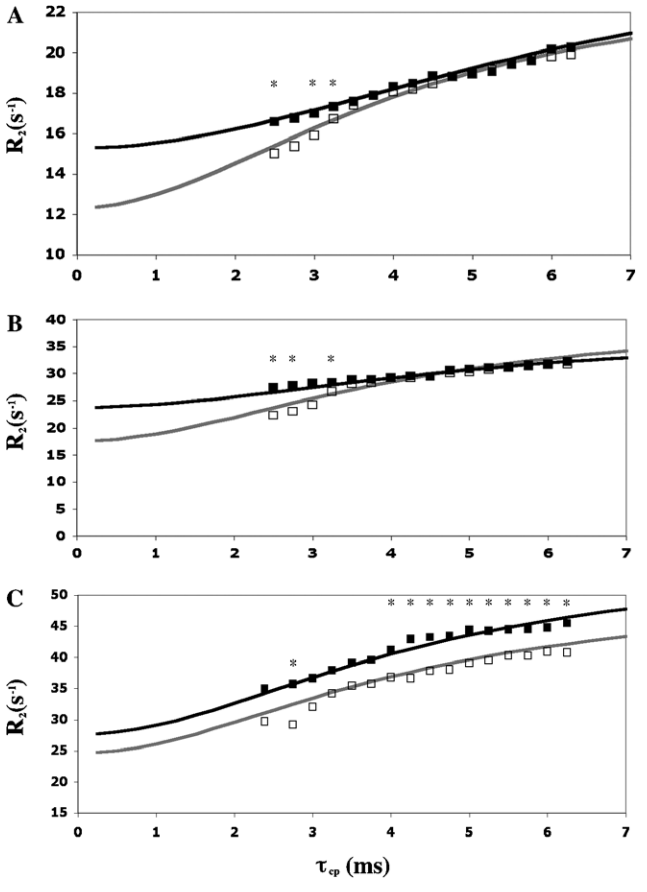

Fig. 3. Estimated transverse relaxation rate values for all phantoms (A, phantom 1; B, phantom 2; C, phantom 3). LASER $R_2^\dagger$ estimates (solid squares) and CPMG R_2 estimates (open symbols) are shown with three-parameter fits of the CE model indicated (LASER, black line and CPMG, gray line). Data uncertainty derived from mono-exponential fit quality is too small to be visible on the plots. Asterisks represent relaxation rate differences ($p < 0.05$).

Table 2
CE Model Fit of experimental results

Phantom	τ_{ex} (ms)	R_{20} (s^{-1})	R_{2D} (s^{-1})
1	2.50 (2.50–3.54)[a]	16.62 (16.56–18.49)	15.95 (13.29–18.61)
2	2.70 (2.70–2.90)	20.69 (20.60–21.27)	19.25 (16.03–25.66)
3	2.50 (2.50–4.19)	24.61 (24.61–27.21)	28.93 (24.80–33.06)

[a] Numbers in brackets represent 95% confidence interval estimated by staged regression analysis [37].

agreement with the predictions of CE theory listed in Table 1 for both R_{20} and R_{2D} (in most cases within experimental uncertainty). Both R_{20} and R_{2D} estimates agreed within 8% for all phantoms, with the exception of the R_{2D} estimate for phantom 1 which exceeded the theoretical prediction slightly beyond experimental uncertainty.

In Fig. 3 for phantoms 1 and 2, the R_2 and $R_2^\dagger$ estimates obtained using CPMG and LASER acquisitions, respectively, converged for larger τ_{cp} values (greater than 3.5 ms), but differed significantly for low τ_{cp} values (statistical significance at 95% confidence level or $p < 0.05$ is indicated by a star above the data points in Fig. 3). For phantom 3, the difference between R_2 and $R_2^\dagger$ estimates obtained from each pulse sequence was present for the full range of τ_{cp} values employed. Using Eq. (3) and the differences between R_2 and $R_2^\dagger$ estimates obtained with CPMG and LASER acquisitions, respectively, the contribution of $R_{2\rho}$ was estimated for each phantom with results shown in Fig. 4 as a function of $\Delta\omega_{ab}^2$. According to Eqs. (4) and (5), the exchange induced contribution to $R_{2\rho}$ ($R_{2\rho,ex}$, Eq. (4)) is proportional to the slope, while the $R_{2\rho}$ contribution resulting from dipolar interactions is given by the intercept ($R_{2\rho,dd}$, Eq. (4)). The theoretical prediction for the slope of the line indicated in Fig. 4 was 5.27×10^{-4} s. The theoretical prediction of the slope ($F_a F_b \tau_{ex} \cos^2\alpha$) was derived from Eqs. (4) and (5), and calculated from parameters associated with properties of the bead phantoms (F_a, F_b, and τ_{ex}) from Eq. (2) and the adiabatic refocusing pulse pattern (α) employed. The experimentally determined slope from Fig. 4 was $(5.18 \pm 0.75) \times 10^{-4}$ s, which agreed within 2% of theoretical predictions and was well within experimental uncertainty.

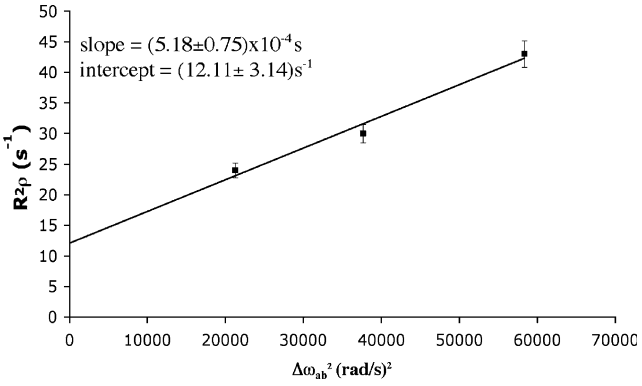

Fig. 4. $R_{2\rho}$ estimates obtained from all three phantoms plotted as a function of chemical shift difference. The slope of the line indicates $R_{2\rho,ex}$ and the intercept- indicates $R_{2\rho,dd}$ (see Eqs. (4) and (5)).

5. Discussion

The main goals of this study were to (1) compare the accuracy of R_2 relaxation rate predictions from the CE model with experimental data acquired from a controlled phantom model of magnetized particles using a conventional CPMG sequence, (2) compare R_2 relaxation rates measured using the LASER pulse sequence to those acquired using the CPMG sequence, and (3) determine whether the CE model, modified to account for $T_{2\rho}$ (or $R_{2\rho}$) relaxation, adequately describes the R_2 relaxation rates measured using LASER under particular experimental conditions. In all cases, our analysis was confined to spherical magnetic perturbers satisfying the weak field regime ($\tau_{ex} < \Delta\omega_{ab}^{-1}$). To achieve this condition in vitro, ORGASOL polyamide microspheres were suspended in Gd-DTPA solutions. Water molecules diffusing amongst the microspheres experience local field inhomogeneity which induces relaxation that can be mimicked by a two-site exchange mechanism. As expected, the relaxation rates measured by the CPMG and LASER sequences were dependent on the susceptibility difference ($\Delta\chi_{ab}$) between the medium and the microspheres, and the time between refocusing pulses ($2\tau_{cp}$). The measured relaxation rates were also dependent on the concentration of Photo-Flo.

To compare CE model R_2 relaxation rate predictions for bead suspension phantoms with experimental data acquired using a conventional CPMG sequence, R_{20} was first calibrated using phantoms without beads but with matched Gd-DTPA and surfactant concentration to control for R_2 variations resulting from these sources. The surfactant Photo-Flo was essential to eliminate air and suspend the polystyrene beads in the agarose gel solution. The R_{20} relaxation rate was calibrated by estimating the relaxivity of Gd-DTPA (c) and the relaxation rate from all other mechanisms including Photo-Flo (y), according to Eq. (6). CPMG and LASER estimates for c and y in Eq. (6) were within experimental error (6.65 ± 0.73 L mmol^{-1} s^{-1} and 10.65 ± 1.57 s^{-1}, respectively, measured with CPMG, and 7.26 ± 0.45 L mmol^{-1} s^{-1} and 11.83 ± 0.98 s^{-1}, respectively, measured with LASER), although the LASER parameter estimates were ~10% higher likely due to the different refocusing pulses used (adiabatic vs. Shinnar-Le Roux) and small refocusing errors at the edge of each selected slice during the localized LASER sequence. The slice selective nature of the last six AFP pulses in the LASER pulse train could also give rise to artifacts by the excitation of signal from outside of the selected volume, in comparison with the completely non-selective CPMG approach. However, the agreement of the measured relaxation rates in bead-free phantoms provides evidence that the refocusing of signal from outside the voxel of interest is not a major source of error.

The CE model [21] has previously been validated for spheres by numerical simulation [25], suggesting good agreement in the weak field regime ($\tau_{ex} < \Delta\omega_B^{-1}$) of the chemical exchange. Simulations of paramagnetic cylinders

(capillaries) by Kennan et al. [12] and vascular beds by Boxerman et al. [34] in the weak field regime were also well fit by the CE model. In the current study, a conventional CPMG pulse sequence was used to measure R_2 relaxation in vitro and showed the expected pattern of variation as a function of the time between refocusing pulses (Fig. 3). Based on the constituents of each phantom in the current study (bead size, volume fraction, [Gd-DTPA]), and using the CE model (Eqs. (1) and (2)), values for τ_{ex}, and R_{2D} were calculated from theory and R_{20} from experimental calibration using bead-free phantoms. Fitting the CE model to the experimental CPMG data produced an R_{2D} value that was overestimated for phantom 1, and a τ_{ex} value that was underestimated for phantom 2, beyond experimental uncertainty, compared to the theoretical predictions. However, for all other estimates, the CE parameters (R_{2D}, R_{20}, and τ_{ex}) derived from the fits to the experimental CPMG data were found to be in close agreement (within experimental uncertainty) with CE model predictions, providing further support for the validity of CE theory predictions for weak spherical magnetic perturbers.

The close agreement between the CE model predictions and the parameter values obtained by fitting the CPMG measured R_2 dependence on τ_{cp} with the CE model was achieved despite using only a finite τ_{cp} range. Under ideal conditions, the curves shown in Fig. 3 would span the entire τ_{cp} range from $\tau_{cp} \ll \tau_{ex}$ to $\tau_{cp} \gg \tau_{ex}$. However the minimum time between refocusing pulses ($2\tau_{cp}$) achievable with the LASER pulse sequence was 5.0 ms, and at the maximum time used between refocusing pulses (12.5 ms), the spin-echo had decayed to the level of the noise at long echo times (i.e., TE $\sim$ 150 ms). Despite experimental limitations on the range of available τ_{cp} values, the near unity R^2-value associated with the linear regression of the signal decay curves (Fig. 2), and the agreement between the transverse relaxation rate parameters (R_{20} and R_{2D}) measured using the CPMG sequence and the values predicted by the CE model, attest to the appropriate application of the CE model theory to estimate relaxation from weak spherical magnetic particle phantoms.

Alternatively to the CE model, variation in transverse relaxation rate (R_2) as a function of τ_{cp} in the weak field regime has also been modeled by Jensen and Chandra as a diffusion rather than an exchange process [24]. Numerical simulations of ^{1}H relaxation rate enhancements from point dipoles calculated by Muller et al. [35] and experimental data obtained from red blood cell suspensions are consistent with diffusion model predictions [24]. However, the two models differ only in how predictions of R_2 transition from the short echo to the long echo (small τ_{cp} vs. large τ_{cp}), and not in the estimated amplitude of the change (i.e., R_{2D} is the same for each model). Despite the similarities of the two models, the results of Jensen and Chandra cannot be synthetized with a simple formula like Eq. (1), which emphasizes the utility of the CE model.

The LASER pulse sequence developed by Garwood and Delabarre [16] was also used to measure $R_2^\dagger$, and has previously been applied in vivo to measure ^{1}H metabolite transverse relaxation times [17] and extended to imaging to measure $R_2^\dagger$ in gray matter, white matter, and CSF [18–20]. However $R_2^\dagger$ measurements made with LASER have not previously been validated in phantom models. In phantoms 1 and 2, results indicated that LASER $R_2^\dagger$ measurements were similar to CPMG when τ_{cp} values were >3.5 ms. However, at lower τ_{cp} values, LASER tended to overestimate R_2 relative to CPMG measurements leading to the overestimation of R_{20} compared to CE model predictions. The observed differences can be explained by the presence of an additional mechanism of contrast, namely $R_{2\rho}$ relaxation as previously reported by Michaeli et al., and described by Eqs. (3)–(5). Predictions from Eq. (3) show that at low τ_{cp} values ($2\tau_{cp} \sim T_p$), an enhanced relaxation resulting from $R_{2\rho}$ mechanisms will contribute significantly to the measured $R_2^\dagger$, while a diminished relaxation enhancement will be observed at larger τ_{cp} values ($2\tau_{cp} \gg T_p$), as demonstrated experimentally in the current study by the similarity between transverse relaxation rate estimates obtained using CPMG and LASER (Fig. 3). Differences in LASER and CPMG R_2 estimates were observed in phantom 3 for the full range of τ_{cp} values used. This difference most likely occurred because phantom 3 has sufficient Gd-DTPA concentration such that it did not strictly satisfy the weak field regime condition ($\tau_{ex} < \Delta\omega_B^{-1}$, with τ_{ex} of 0.0031 s^{-1} and $\Delta\omega_B^{-1}$ of 0.0033 s^{-1}) and would more appropriately be categorized as within the intermediate exchange regime ($\tau_{ex} \sim \Delta\omega_B^{-1}$). This difference between LASER and CPMG R_2 estimates was consistently observed for 3 separate preparations of the phantom 3 suspension, and emphasizes the importance of limiting $R_{2\rho}$ predictions from LASER measurements to applications involving the weak exchange regime.

To determine whether the effect of $R_{2\rho}$ relaxation could account for the observed differences between LASER and CPMG at low values of τ_{cp}, the $R_{2\rho}$ relaxation rates were calculated using Eqs. (3)–(5). Since the only difference between phantoms was the concentration of Gd-DTPA ($\Delta\chi_{ab}$), only the $R_{2\rho,ex}$ parameter was predicted to vary between phantoms (Eq. (4)). The calculated $R_{2\rho}$ relaxation rates were plotted as a function of chemical shift difference ($\Delta\omega_{ab}$) for all three phantoms (Fig. 4) to isolate the contribution of $R_{2\rho,ex}$ (slope) and $R_{2\rho,dd}$ (intercept). The slope of the line in Fig. 4 ($(5.18 \pm 0.75) \times 10^{-4}$ s^{-1}) represents $R_{2\rho,ex}$ and agreed within error with the value predicted by theory (5.27×10^{-4} s^{-1}) (determined using $F_a F_b \tau_{ex} \cos^2\alpha$, Eq. (5)) based on Eqs. (1)–(7) in Michaeli et al. [20]. This result suggests that the differences between LASER and CPMG transverse relaxation rate estimates can be explained by the $R_{2\rho}$ contrast enhancement mechanism. Therefore, we have demonstrated a theoretical basis for the differences in transverse relaxation rates observed between LASER and CPMG at small τ_{cp} values involving weak magnetic perturbers.

The LASER pulse sequence is ideally suited for in vivo applications that require localized excitation, since

exclusively adiabatic pulses are used, which are relatively insensitive to B_1-inhomogeneity. Additionally, LASER can produce diffusion sensitive contrast around micro field inhomogeneities. The observed hyper-sensitivity of LASER to diffusion contrast at short τ_{cp} combined with the quantitative accuracy of the enhancement based on the theory described by Michaeli et al. [11], and confirmed experimentally with weak magnetic particle suspensions in this work, suggests the LASER pulse sequence may eventually provide a means to detect stored iron in brain disorders, and hemochromatosis in liver. Quantitative measures of iron content could be derived using the experimental confirmation of $T_{2\rho}$ theory for applications well approximated by the spherical particle weak perturber model, the most likely case for small in vivo ferritin deposits associated with many types of pathology.

6. Conclusion

In this study, ORGASOL polyamide microspheres suspended in Gd-DTPA solutions were used to control magnetic susceptibility in three phantoms and simulate in vivo conditions. The LASER $R_2^{\dagger}$ measurements in the calibration phantoms containing no ORGASOL microspheres agreed with the CPMG R_2 measurements. The transverse relaxation rate parameters (R_{20} and R_{2D}) derived from the CPMG fits were found to be in good agreement with CE theory predictions. LASER $R_2^{\dagger}$ values were found to be in agreement with the CPMG pulse sequence for high τ_{cp} values (>3.5 ms), however significant discrepancies were observed between the two sequences at low τ_{cp} values (<3.5 ms). The differences between the two were attributed to the presence of $R_{2\rho}$ relaxation in a fashion predicted by theory. This property may be exploited in future in vivo studies that use LASER to quantify transverse relaxation in pathological conditions (stroke, Parkinson's disease, hereditary hemochromatosis). The observed relaxation rate dependence on τ_{cp} could be exploited to selectively weight signal from tissue regions containing small magnetic particles [36], and potentially identify and quantify the presence of cells that are labeled with iron oxide particles (i.e., MION).

Acknowledgments

The authors wish to thank Dr. Michael Garwood for providing the LASER spectroscopy sequence. Funding provided by the National Institutes of Health Research (R01-EB001852) and the Canadian Institutes of Health Research (MME-15594).

References

[1] R. Ordidge, J. Gorell, J. Deniau, R. Knight, J. Helpern, Assessment of relative brain iron concentrations using T_2-weighted and T_2* weighted MRI at 3 Tesla, Magn. Reson. Med. 32 (1994) 335–341.

[2] Y. Gossuin, A. Roch, R. Muller, P. Gillis, Relaxation induced by ferritin and ferritin like magnetic particles: the role of proton exchange, Magn. Reson. Med. 43 (2000) 237–243.

[3] R. Brooks, J. Vymazal, J. Bulte, C. Baumgarner, V. Tran, Comparison of T_2 relaxation in blood, brain and ferritin, J. Magn. Reson. Imaging 4 (1995) 446–450.

[4] F. Ye, W. Martin, P. Allen, Estimation of the iron concentration in excised gray matter by means of proton relaxation measurements, Magn. Reson. Med. 35 (1996) 285–289.

[5] K. Whyttall, A. MacKay, D. Graeb, R. Nugent, D. Li, D. Paty, In vivo measurements of distributions and water contents in normal human brain, Magn. Reson. Med. 37 (1997) 34–43.

[6] J. Jensen, R. Chandra, Theory of nonexponential NMR signal decay in liver with iron overload or superparamagnetic iron oxide particles, Magn. Reson. Med. 47 (2002) 1131–1138.

[7] Z.M. Quian, Q. Wang, Expression of iron transport proteins and excessive iron accumulation in the brain in neurodegenerative disorders, Brain Res. Rev. 27 (1998) 257–267.

[8] A.G. Anderson, R.L. Garwin, E.L. Hahn, J.W. Horton, G.L. Tucker, R.M. Walker, Spin echo serial storage memory, J. Appl. Phys. 26 (1953) 1324–1338.

[9] H.Y. Carr, E.M. Purcell, Effects of diffusion on free precession in nuclear magnetic resonance experiments, Phys. Rev. 94 (1954) 630–638.

[10] S. Meiboom, D. Gill, Modified Spin-Echo method for measuring nuclear relaxation times, Rev. Sci. Instrum. 29 (1958) 688–691.

[11] S. Michaeli, H. Grohn, O. Grohn, D. Source, R. Kauppinen, C.S. Springer, K. Ugurbil, M. Garwood, Exchange influenced $T_{2\rho}$ contrast in human brain images measured with adiabatic radio frequency pulses, Magn. Reson. Med. 53 (2005) 823–829.

[12] R. Kennan, J. Zhong, J. Gore, Intravascular susceptibility contrast mechanisms in tissues, Magn. Reson. Med. 31 (1994) 9–21.

[13] A. Sorensen, A. Tievski, L. Ostergaard, R. Weisskoff, B. Rosen, Contrast agents in functional MR imaging, J. Magn. Reson. Imaging 37 (1997) 530–536.

[14] R. Weisskoff, C. Zuo, J. Boxerman, B. Rosen, Microscopic susceptibility variation and transverse relaxation: theory and experiment, Magn. Reson. Med. 31 (1994) 601–610.

[15] R. Mathur-DeVre, M. Lemort, Invited review: biophysical properties and clinical applications of magnetic resonance imaging contrast agents, Br. J. Radiol. 68 (1995) 225–247.

[16] M. Garwood, L. DelaBarre, The return of the frequency sweep: designing adiabatic pulse for contemporary NMR, J. Magn. Reson. 153 (2001) 155–177.

[17] S. Michaeli, M. Garwood, X.H. Zhu, L. DelaBarre, P. Andersen, G. Adriani, H. Merkle, K. Ugurbil, W. Chen, Proton T_2 relaxation study of water, *N*-acetylaspartate and creatine in human brain using Hahn and Carr–Purcell spin echoes at 4T and 7T, Magn. Reson. Med. 47 (2002) 629–633.

[18] R. Bartha, S. Michaeli, H. Merkle, et al., In vivo $1H_20$ T_2 measurement in the human occipital lobe at 4T and 7T by Carr–Purcell MRI: detection of microscopic susceptibility contrast, Magn. Reson. Med. 47 (2002) 1–8.

[19] M. Kavec, O.H. Grohn, H.I. Grohn, M. Garwood, R.A. Kauppinen, Dynamic dephasing in developing ischemic cerebral infarction in rats studied by Carr–Purcell T_2 magnetic resonance imaging, Magn. Reson. Med. 53 (2005) 960–964.

[20] S. Michaeli, D. Source, D. Idiyatullin, K. Ugurbil, M. Garwood, Transverse relaxation in the rotating frame induced by chemical exchange, J. Magn. Reson. 169 (2004) 293–299.

[21] A. Brooks, F. Moiny, P. Gillis, On T_2 shortening by weakly magnetized particles: the chemical exchange model, Magn. Reson. Med. 45 (2001) 1014–1020.

[22] R. Brown, P. Fantazzinni, Conditions for initial quasilinear T_2^{-1} versus τ for Carr–Purcell- Meiboom-Gill NMR with diffusion and susceptibility differences in porous media and tissues, Phys. Rev. B 47 (1993) 14823–14834.

[23] Z. Luz, S. Meiboom, Nuclear magnetic resonance study of the protolysis of trimethylammonium ion in aqueous solution-order of

the reaction with respect to solvent, J. Chem. Phys. 39 (1963) 366–370.
[24] J. Jensen, R. Chandra, NMR relaxation in tissues with weak magnetic inhomogeneities, Magn. Reson. Med. 44 (2000) 144–156.
[25] F. Moiny, P. Gillis, A. Roch, R. Muller, Transverse relaxation of superparamagnetic contrast agents: a numerical analysis, In Proc. 11th Annual Meeting SMRM, Works in Progress, 1002 1431.
[26] A. Tannus, M. Garwood, Improved performance of frequency-swept pulses using offset independent adiabaticity, J. Magn. Reson. Imaging 120 (1996) 133–147.
[27] M. Silver, R. Joseph, D. Hoult, Highly selective $\pi/2$ and π pulse generation, J. Magn. Reson. 59 (1998) 347–351.
[28] T. Gullion, New compensated Carr–Purcell sequences, J. Magn. Reson. 89 (1990) 479–484.
[29] E. Hendrick, M. Haake, Basic physics of MR contrast agents and maximization of image contrast, J. Magn. Reson. Imaging 3 (1993) 137–148.
[30] C. Bowen, X. Zhang, J. Saab, P. Gareau, Application of the static dephasing regime theory to superparamagnetic iron-oxide loaded cells, Magn. Reson. Med. 48 (2002) 52–61.
[31] R. Weisskoff, S. Kihne, MRI susceptometry: image based measurement of absolute susceptibility of MR contrast agents and human blood, Magn. Reson. Med. 24 (1992) 375–383.
[32] S. Chu, Y. Xu, J. Balschi, C. Springer, Bulk magnetic susceptibility shifts in NMR studies of compartmentalized samples: use of paramagnetic reagents, Magn. Reson. Med. 46 (1990) 239–262.
[33] K. Whittal, A. MacKay, Quantitative interpretation of NMR relaxation data, J. Magn. Reson. 84 (1989) 134–152.
[34] J. Boxerman, L. Hamberg, B. Rosen, R. Weisskoff, MR contrast due to intravascular magnetic susceptibility perturbations, Magn. Reson. Med. 34 (1995) 555–566.
[35] R. Muller, P. Gillis, F. Moiny, A. Roch, Transverse relaxivity of particulate MRI contrast media: from theories to experiments, Magn. Reson. Med. 22 (1991) 178–182.
[36] L. Stables, P. Kennan, J. Gore, Assymetric spin echo imaging of magnetically inhomogeneous systems: theory, experiment, and numerical studies, Magn. Reson. Med. 40 (1998) 432–442.
[37] N.R. Draper, H. Smith, Applied Regression Analysis, John Wiley & Sons, New York, 1981.